Front. Phys., 2013, 8(1): 44–49
DOI 10.1007/s11467-013-0290-3

RESEARCH ARTICLE

Strong localization across the metal–insulator transition at the Ag/Si(111)-($\sqrt{3} \times \sqrt{3}$)R30° interface

Yuan-Yuan Tang, Jian-Dong Guo†

Beijing National Laboratory for Condensed Matter Physics & Institute of Physics, Chinese Academy of Sciences, Beijing 100190, China

E-mail: †jdguo@iphy.ac.cn

Received January 5, 2013; accepted January 14, 2013

We present the temperature dependent electrical transport measurements of Ag/Si(111)-($\sqrt{3} \times \sqrt{3}$)R30° by the *in situ* micro-four-point probe method integrated with scanning tunneling microscopy. The surface structure characterizations show hexagonal patterns at room temperature, which supports the inequivalent triangle (IET) model. A metal–insulator transition occurs at ∼115 K. The low temperature transport measurements clearly reveal the strong localization characteristics of the insulating phase.

Keywords surface conductivity, metal–insulator transition, localization, scanning tunneling microscopy

PACS numbers 73.25.+i, 73.50.-h, 73.20.Fz, 68.37.Ef

1 Introduction

The development of nanodevices calls for intense attention to the studies of electronic transport of materials in reduced dimensionalities, which might be dictated by different quantum mechanics as compared to that in their three dimensional forms. Ultra-thin metal films on semiconductor substrates have been a playground for the study of electronic transport properties of low dimensional materials [1–5], since normally the energy bands in the semiconducting substrates are away from the Fermi level (E_F) of the system and therefore the electrons do not interfere with the transport in the metal films. Low dimensional metals at their two-dimensional extremes can be achieved in the systems of monolayered (or even submonolayered) metals on semiconductors, i.e., the metal/semiconductor interfaces. In such systems, detailed information of both lattice and band structures is necessary for the understanding of the transport properties because they are the most important factors that determine the electron density of states (DOS) at E_F.

Ag/Si(111)-($\sqrt{3} \times \sqrt{3}$)R30° (referred to as $\sqrt{3}$-Ag in the following) is a typical two dimensional electron system. Atom arrangements of $\sqrt{3}$-Ag have been studied by both experimental observations and theoretical calculations [6–10]. The generally accepted model was the honeycomb chained triangle (HCT) model, in which one Si trimer is surrounded by three Ag atoms that are equally located at the corners of the honeycombs, appearing as the honeycomb patterns in room temperature (RT) scanning tunneling microscopy (STM) [9, 10]. Recently, hexagonal patterns at low temperature (LT) have been observed, which was attributed to the inequivalent triangle (IET) structure with a lower total energy than that of the HCT structure [6, 7]. The $\sqrt{3}$-Ag surface changes from the symmetric HCT structure to the asymmetric IET structure at 150 K [11, 12]. However, whether this is a structural phase transition is still under debate. It has been proposed that the HCT structure might not be static and the observed honeycomb pattern at RT could be the mixture of IET+ and IET– structure [11, 13, 14].

Although the scanning tunneling spectroscopy (STS) investigations revealed the nearly free-electron-like two-dimensional metallic surface state (S_1) [7], photoemission spectroscopy observed the surface bands (S_2 and S_3) arising from the IET structure, suggesting the asymmetric characteristics of $\sqrt{3}$-Ag [11]. Detailed studies also pointed out that the electronic properties of $\sqrt{3}$-Ag sensitively depend on electron doping – the stoichiometric

$\sqrt{3}$-Ag surface with exactly one monolayer (ML) of Ag atom is semiconducting [15], while adsorption of monovalent metals, such as noble metals (Ag, Au) or alkali metals (K, Cs), can dope electrons into the surface band S_1 and therefore cause metallization of the system [15–17]. Crain *et al.* further pointed out that Ag adsorption caused not only the simple electronic doping but also the move-down of the surface band bottom into the valence band [18].

The metallization caused by adsorption of metal atoms on $\sqrt{3}$-Ag results in a steep increase of electric conductance as detected by four-probe measurements [15, 19]. Recently, Matsuda *et al.* measured the conductivity of ∼1 ML $\sqrt{3}$-Ag with the surface sensitive micro-four-point probe (MFPP) method and reported the metal–insulator transition (MIT) occurring at ∼150 K [20]. They proposed that the LT electric transport could be attributed to strong localization of electrons in the surface states due to random potential enhanced by standing waves created around surface defects. Liu *et al.* further studied the temperature-dependent electrical conductance (110–300 K) by intentionally introducing defects by depositing additional Au atoms on the $\sqrt{3}$-Ag surface [21]. But with 0.02 ML Au atoms deposited on the surface, they observed weak localization effect below 180 K. To clarify the picture of the localization across the MIT on $\sqrt{3}$-Ag, electrical transport data at lower temperatures are required.

In this paper, we report the measurements of electric conductance of Ag-adsorbed $\sqrt{3}$-Ag surface as a function of temperature (77–270 K) by *in situ* MFPP as well as STM characterizations. Our occupied-state STM images show hexagonal patterns at RT, supporting the IET model without structural phase transition. The temperature dependent resistivity indicates the MIT occurring at around 115 K. The data in a broad temperature range clearly reveal the strong localization characteristics of the LT transport.

2 Experiments

The experiments were performed in an ultrahigh vacuum (UHV) chamber with the base pressure of 1×10^{-10} Torr. We used n-type Si (P-doped) substrates with the RT resistivity of 5 Ω·cm. The samples were prepared in UHV by direct current heating up to 1250 °C. The LEED patterns showed that the (7×7) reconstruction is formed on Si(111) surface. Then 1 ML Ag was deposited at the rate of 0.025 ML/min for 45 min (1 ML=7.84×10^{14} cm^{-2}) followed by annealing at 550 °C for 3 min to form the $(\sqrt{3}\times\sqrt{3})$R30° reconstruction. The sample temperature was monitored by an infrared pyrometer. After the sample was cooled down to RT, we deposited additional 0.05 ML Ag atoms as dopants. The STM characterizations were carried out with an LT STM (Omicron). The STM tips were made from a W wire.

Electric transport measurements on low dimensional metal systems are technically difficult since they are chemically active and only survive in UHV environments. Besides, surface-sensitive methods are required to avoid the substrate effects that could be coupled with the transport of the metal systems atop. Several methods, including monolithic MFPP and independently driven four-tip STM probes, have been developed to fulfil the task [22–26]. Here we used the monolithic MFPP method integrated with our LT STM. As shown in Fig. 1(a), four electrodes were made on the standard STM scanning head, connecting to the external measurement circuit. The standard tip carrier was modified by attaching a BeCu spring in the middle of the three gold-coated poles [Fig. 1(b)]. This modified ceramic probe carrier was interchangeable with the standard tip carrier in UHV, and made the electric contacts between the four electrodes on scanning head and those on the probe carrier (the three poles and the spring), respectively. A 30° ceramic slope was fixed on the other side of the probe carrier, hosting the four-probe chip [Fig. 1(c)]. In the current work, two types of probe chips were used. One was the commercial type from Capres Corpoartion [27]. The other was made of four Au wires attached separately on a ceramic plate. Taking the advantage of STM preamplifier, the probe chip could be driven to the sample surface automatically with tunneling current (I_t) as the feedback signal. After the stable tunneling between the probe and sample was detected, the amplifier was turned off and a few more steps were applied to the STM coarse motor for approaching until all the probes got good contacts to the surface. The conductivity was measured with standard four-probe scheme in which the current flowing through the outer pair of probes (I) was swept while the voltage drop between the inner pair of probes (V) was recorded. The integration of the MFPP with LT STM also allowed the vibration-proof environments and a broad temperature range (4–300 K) for transport measurements.

3 Results and discussion

3.1 STM characterizations

Since the appearance of 6×1 phase on $\sqrt{3}$-Ag surface signals that no excess Ag atoms is doped [28], we obtain the stoichiometric $\sqrt{3}$-Ag by gradually increasing the Ag deposition dosage to minimize the ratio of 6×1 phase. Figure 2 (a) shows the STM image of the $\sqrt{3}$-Ag surface

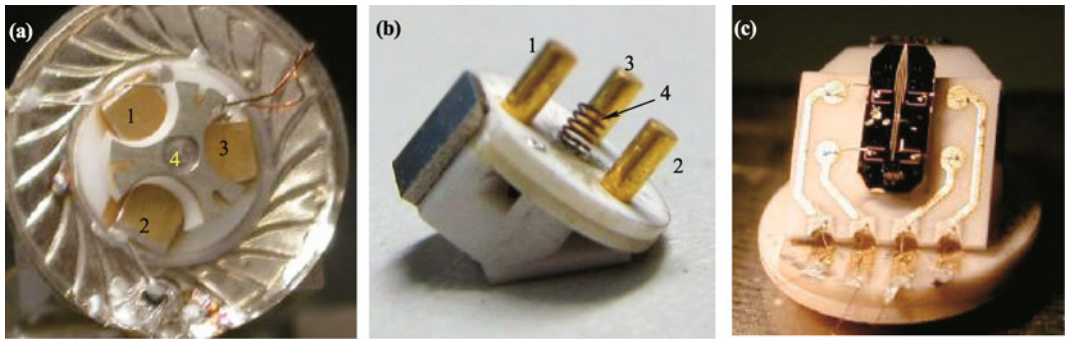

Fig. 1 **(a)** STM head with four electrodes (Omicron standard). **(b)** The ceramic probe carrier with three golden legs and a spring leg at the center. **(c)** The ceramic probe carrier with an MFPP chip attached.

at RT. Only a tiny amount (less than 0.1% area ratio) of 6×1 phase can be found near the step edges (not shown here). Then we intentionally deposit additional 0.05 ML Ag on the surface. Those Ag atoms act as 2D adatom gas (2DAG) at RT [29] and do not change STM images or LEED patterns at all.

In the unoccupied-state STM image [Fig. 2(b)], the $\sqrt{3}$-Ag surface shows a honeycomb pattern with two identical bright features in each unit cell. However, the occupied-state STM image [Fig. 3(c)] clearly shows two different types of protrusions forming a hexagonal pattern. This is inconsistent with the HCT model, in which the distribution of electron DOS within a $(\sqrt{3} \times \sqrt{3})$ unit cell should have been symmetric. With STS investigations, Zhang *et al.* have claimed that the electronic structures of the RT and LT phases of $\sqrt{3}$-Ag are similar [30]. In the current work, the asymmetric DOS distribution in a unit cell observed at RT is also identical to that at LT [6, 8]. Therefore we conclude that there is no HCT-IET structural phase transition on $\sqrt{3}$-Ag surface and the asymmetric IET structure can be stabilized at RT.

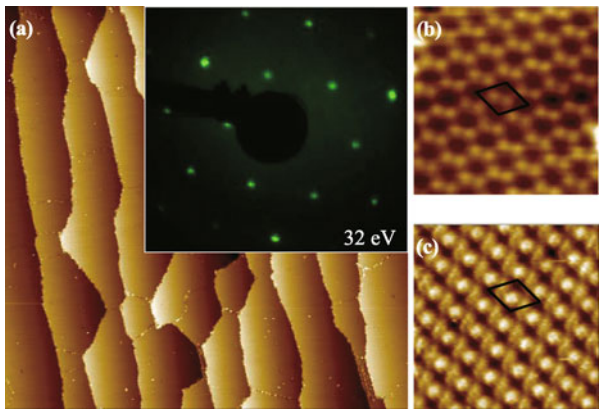

Fig. 2 **(a)** STM image (300×300 nm^2, –1.8V/100pA) of the stoichiometric $\sqrt{3}$-Ag surface at RT. Inset is the LEED patterns at 32 eV. **(b)** and **(c)** High-resolution STM images (3 × 3 nm, 10 pA) taken with the bias at 0.4 V and –0.5 V, respectively. The surface unit cell is indicated by the rhombuses.

3.2 Conductivity measurements

We first check the surface sensitivity of our MFPP method by measuring the resistance of two types of surfaces, i.e., the stoichiometric $\sqrt{3}$-Ag surface and the one doped by 0.05 ML Ag adatoms. Figure 3 shows the I–V curves measured at RT with the probe spacing of 10 μm. Both of them show linear line shape, indicating the resistance of the stoichiometric $\sqrt{3}$-Ag and Ag-doped surfaces as 17.3 kΩ and 2.16 kΩ, respectively. In general, the electric current applied to metal/semicondutor interface flows through three channels in parallel: the surface states, the space charge layer (SCL) and the substrate bulk. In the current work, the E_F of the $\sqrt{3}$-Ag surface locates at 0.16 eV above the bulk valence-band maximum [31]. This leads the SCL to be an inversion layer on the n-type Si substrate, separated by an depletion layer from the bulk [5]. Therefore the measuring current is effectively confined within the surface-state channel and high surface sensitivity is obtained in our MFPP measurements.

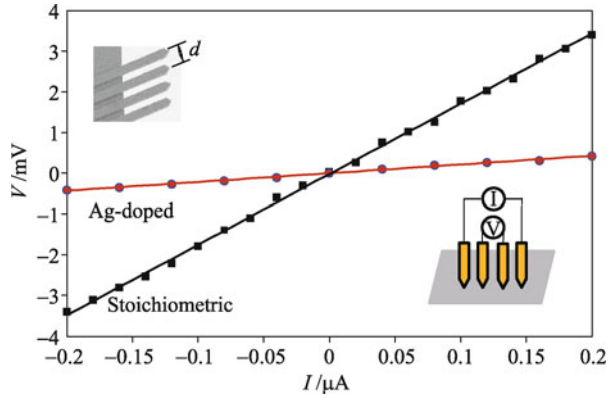

Fig. 3 I–V curves of the stoichiometric $\sqrt{3}$-Ag surface (*black*) and the one doped by 0.05 ML Ag adatoms (*red*) measured by MFPP method at RT.

To further verify the surface sensitivity of our measurements, we compare the resistance of $\sqrt{3}$-Ag measured by probes with different spacing (d). According to Ohm's

law, the resistance of an infinite 2D system measured by the four-point probe is independent of d. We replaced the commercial MFPP chip (d=10 μm) with four Au wires, whose spacing can be adjusted from ∼100 μm to ∼1 mm. The results show no detectable change when $d \leqslant$200 μm, confirming that our MFPP measurements present the electric transport characteristics of the 2D $\sqrt{3}$-Ag system. Since the Au wires are durable against repeated touching-detaching cycles to the sample surface, we use the Au-wire type probes with the spacing of 200 μm in the following experiments.

3.3 Metal–insulator transition

Temperature dependent resistance of the Ag-doped $\sqrt{3}$-Ag surface is measured with the Au-wire probes (d=200 μm) from RT down to 77 K. The data during cooling-down and heating-up processes are collected and the results show no difference. The sheet resistivity (ρ_{2D}) of the surface states is calculated from the measured resistance (R) by $\rho_{2D} = \pi R/\ln 2$ [32], as shown in Fig. 4. Between RT and 170 K, ρ_{2D} exhibits a metallic temperature dependence [$\mathrm{d}\rho(T)/\mathrm{d}T > 0$], while it turns to be insulating below 110 K with a discontinuity point at around 115 K, indicating the occurance of MIT. At intermediate temperatures between 170 K and 115 K, ρ_{2D} barely changes.

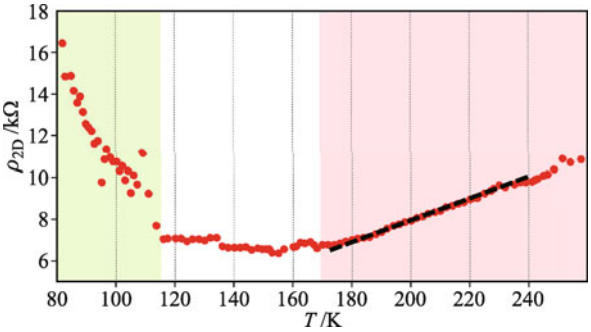

Fig. 4 The temperature dependent sheet resistivity (ρ_{2D}) of Ag-doped $\sqrt{3}$-Ag surface from 270 K to 77 K. The black dashed line from 240 to 170 K shows the fitting results with Eq. (1).

The different temperature dependence of ρ_{2D} in the above three temperature ranges correspond to different electric transport mechanisms. Above 170 K, despite of the interaction between impurity states, the Ag-doped $\sqrt{3}$-Ag surface can still be considered as a free-electron-like 2D metallic system [7]. The temperature dependent sheet resistivity can be fitted to the Boltzmann transport equation:

$$\rho_{2D} = \frac{4\pi^2 m^* \lambda}{\hbar e^2 k_F^2} k_B T \tag{1}$$

where k_B is the Boltzmann constant, λ is electron-phonon coupling constant, m^* is the effective mass, and k_F is the Fermi momentum. The dashed line in Fig. 4 shows the fitting results with Eq. (1), where $m^*/(k_F)^2$ is determined by the angle-resolved photoemission spectroscopy (ARPES) measurements reported by Matsuda *et al.* [20]. The fitting shows that the electron-phonon coupling constant λ=1, larger than that of typical bulk metals (λ=0.1–0.3), but consistent with the previously reported result on $\sqrt{3}$-Ag surface [20].

Below 115 K, the temperature dependence of $\rho(T)$ indicates the insulating characteristics of the electrical transport on $\sqrt{3}$-Ag surface. It is not related to the formation of a band insulator since ARPES measurements showed that the surface band structure remains metallic without energy gap opened at E_F [20]. Moreover, it cannot be directly attributed to the lattice structure either because our STM characterizations do not support the picture of HCT-IET structural transition. Localization theories have been introduced to describe the MIT occurring on the $\sqrt{3}$-Ag surface [20, 21]. Here with the experimental measurements in a broad temperature range, we investigate such a picture in detail. Within the weak localization picture, the conductivity of 2D metals (σ_{2D}) depends on the temperature in the following:

$$\sigma_{2D} = \alpha \cdot \frac{e^2}{2\pi^2\hbar} \cdot \ln T + C \tag{2}$$

where α is the power related to the temperature dependence of the phase relaxation time of the carriers ($\tau_\phi \propto T^{-\alpha}$) and C is a constant. The value of α should be between 1 and 2 in the case of weak localization, far below our fitting result (λ=10.2), as shown in Fig. 5(a). The weak localization picture is not valid to describe the MIT on the Ag-doped $\sqrt{3}$-Ag surface.

The strong localization in 2D metals represented by Mott's variable range hopping (VRH) model calculates σ_{2D} as

$$\sigma_{2D} = \sigma_0 \exp\left(-\left(\frac{\Delta E}{k_B T}\right)^{1/3}\right) \tag{3}$$

where ΔE is the activation energy. As shown in Fig. 5(b), such a model fits the experimental results well. We obtain ΔE=1.1 eV. Then the localization length can be obtained by $\xi = \sqrt{3^3/\pi D_{2D} \Delta E}$, where $D_{2D} = m^*/(\pi\hbar^2)$ is the electron DOS at E_F, which is dependent on the doping level. We use an approximation of $m^* = 0.13 m_e$ [16, 18] and obtain $D_{2D} = 0.54\ \mathrm{eV}^{-1} \cdot \mathrm{nm}^{-2}$, from which the localization length ξ is estimated as ∼38 nm.

Between 170 and 115 K, the temperature dependence of ρ_{2D} does not fit to the Boltzmann model or the localization models. Similar behavior has been reported on the Au-adsorbed $\sqrt{3}$-Ag surface [21]. Such a complicated transport phenomenon might be originated from the

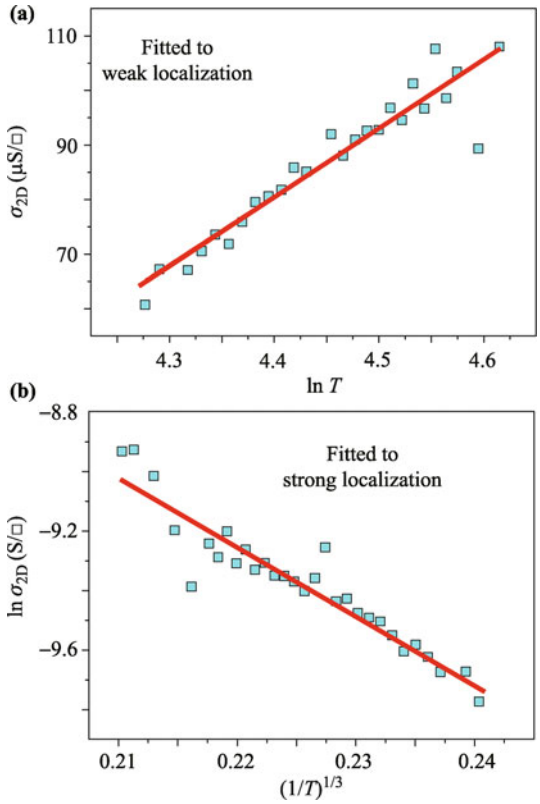

Fig. 5 The temperature dependent ρ_{2D} below 115 K fitted to **(a)** the weak localization theory and **(b)** the strong localization theory, respectively. The experimental data are plotted in scattered points while the fitted results are plotted in solid lines.

interaction between the electronic states of Ag dopants and the intrinsic surface states of $\sqrt{3}$-Ag.

4 Conclusion

In summary, we present both RT STM characterizations and *in situ* MFPP electric transport measurements in a broad temperature range (from RT to 77 K) on the $\sqrt{3}$-Ag surface. Our STM image shows a hexagonal pattern at RT, supporting the IET model without structural phase transition. The temperature dependence of sheet resistance clearly indicates an MIT occurring at 115 K. This MIT can be well described by the strong localization theory with the variable range hopping model.

Acknowledgements We thank Dr. Aizi Jin at the Institute of Physics, CAS, for the technique support. This work was supported by the National Basic Research Program of China (973 Program) (Grant No. 2012CB921700) and Specific Funding of Discipline and Graduate Education Project of Beijing Municipal Commission of Education.

References and notes

1. T. Uchihashi, P. Mishra, M. Aono, and T. Nakayama, Phys. Rev. Lett., 2011, 107(20): 207001
2. S. Yamazaki, Y. Hosomura, I. Matsuda, R. Hobara, T. Eguchi, Y. Hasegawa, and S. Hasegawa, Phys. Rev. Lett., 2011, 106(11): 116802
3. T. Hirahara, I. Matsuda, S. Yamazaki, N. Miyata, S. Hasegawa, and T. Nagao, Appl. Phys. Lett., 2007, 91(20): 202106
4. F. Song, L. Gammelgaard, Ph. Hofmann, and J. W. Wells, Appl. Phys. Lett., 2011, 98(5): 052106
5. T. Tanikawa, I. Matsuda, T. Kanagawa, and S. Hasegawa, Phys. Rev. Lett., 2004, 93(1): 016801
6. H. Aizawa, M. Tsukada, N. Sato, and S. Hasegawa, Surf. Sci., 1999, 429(1–3): L509
7. N. Sato, S. Takeda, T. Nagao, and S. Hasegawa, Phys. Rev. B, 1999, 59(3): 2035
8. Y. Nakamura, Y. Kondo, J. Nakamura, and S. Watanabe, Phys. Rev. Lett., 2001, 87(15): 156102
9. Y. G. Ding, C. T. Chan, and K. M. Ho, Phys. Rev. Lett., 1991, 67(11): 1454
10. S. Watanabe, M. Aono, and M. Tsukada, Phys. Rev. B, 1991, 44(15): 8330
11. I. Matsuda, H. Morikawa, C. Liu, S. Ohuchi, S. Hasegawa, T. Okuda, T. Kinoshita, C. Ottaviani, A. Cricenti, M. D'angelo, P. Soukiassian, and G. L. Lay, Phys. Rev. B, 2003, 68(8): 085407
12. H. Tajiri, K. Sumitani, S. Nakatani, A. Nojima, T. Takahashi, K. Akimoto, H. Sugiyama, X. Zhang, and H. Kawata, Phys. Rev. B, 2003, 68(3): 035330
13. J. W. Wells, J. F. Kallehauge, and Ph. Hofmann, J. Phys.: Condens. Matter, 2007, 19(17): 176008
14. K. J. Wan, X. F. Lin, and J. Nogami, Phys. Rev. B, 2006, 74: 201304(R)
15. Y. Nakajima, S. Takeda, T. Nagao, S. Hasegawa, and X. Tong, Phys. Rev. B, 1997, 56(11): 6782
16. T. Hirahara, I. Matsuda, M. Ueno, and S. Hasegawa, Surf. Sci., 2004, 563(1–3): 191
17. I. Matsuda, T. Hirahara, M. Konishi, C. Liu, H. Morikawa, M. D'angelo, S. Hasegawa, T. Okuda, and T. Kinoshita, Phys. Rev. B, 2005, 71(23): 235315
18. J. N. Crain, M. C. Gallagher, J. L. McChesney, M. Bissen, and F. J. Himpsel, Phys. Rev. B, 2005, 72(4): 045312
19. S. Hasegawa, X. Tong, S. Takeda, N. Sato, and T. Nagao, Prog. Surf. Sci., 1999, 60(5–8): 89
20. I. Matsuda, C. Liu, T. Hirahara, M. Ueno, T. Tanikawa, T. Kanagawa, R. Hobara, S. Yamazaki, S. Hasegawa, and K. Kobayashi, Phys. Rev. Lett., 2007, 99(14): 146805
21. C. Liu, I. Matsuda, S. Yoshimoto, T. Kanagawa, and S. Hasegawa, Phys. Rev. B, 2008, 78(3): 035326
22. S. Hasegawa, I. Shiraki, F. Tanabe, R. Hobara, T. Kanagawa, T. Tanikawa, I. Matsuda, C. L. Petersen, T. M. Hansen, P. Boggild, and F. Grey, Surf. Rev. Lett., 2003, 10(06): 963

23. N. Miyata, R. Hobara, H. Narita, T. Hirahara, S. Hasegawa, and I. Matsuda, Jpn. J. Appl. Phys., 2011, 50: 036602
24. T. Tanikawa, I. Matsuda, R. Hobara, and S. Hasegawa, Surf. Sci. Nanotechnol., 2003, 1: 50
25. S. Hasegawa and F. Grey, Surf. Sci., 2002, 500(1–3): 84
26. R. Hobara, N. Nagamura, S. Hasegawa, I. Matsuda, Y. Yamamoto, Y. Miyatake, and T. Nagamura, Rev. Sci. Instrum., 2007, 78(5): 053705
27. http://www.capres.com
28. M. Ueno, I. Matsuda, C. Liu, and S. Hasegawa, Jpn. J. Appl. Phys., 2003, 42: 4894
29. Y. Nakajima, G. Uchida, T. Nagao, and S. Hasegawa, Phys. Rev. B, 1996, 54(19): 14134
30. H. M. Zhang, J. B. Gustafsson, and L. S. O. Johansson, Phys. Rev. B, 2006, 74: 201304(R)
31. X. Tong, C. S. Jiang, and S. Hasegawa, Phys. Rev. B, 1998, 57(15): 9015
32. P. A. Lee and T. V. Ramakrishnan, Rev. Mod. Phys., 1985, 57(2): 287